

This work was written as part of one of the author's official duties as an Employee of the United States Government and is therefore a work of the United States Government. In accordance with 17 U.S.C. 105, no copyright protection is available for such works under U.S. Law.

Public Domain Mark 1.0

<https://creativecommons.org/publicdomain/mark/1.0/>

Access to this work was provided by the University of Maryland, Baltimore County (UMBC) ScholarWorks@UMBC digital repository on the Maryland Shared Open Access (MD-SOAR) platform.

Please provide feedback

Please support the ScholarWorks@UMBC repository by emailing scholarworks-group@umbc.edu and telling us what having access to this work means to you and why it's important to you. Thank you.

Cirrus optical depth and lidar ratio retrieval from combined CALIPSO-CloudSat observations using ocean surface echo

Damien Josset,¹ Jacques Pelon,² Anne Garnier,² Yongxiang Hu,³ Mark Vaughan,³ Peng-Wang Zhai,¹ Ralph Kuehn,⁴ and Pat Lucker¹

Received 13 October 2011; revised 9 January 2012; accepted 13 January 2012; published 8 March 2012.

[1] Ocean surface observations from the CloudSat radar and the spaceborne lidar aboard the Cloud Aerosol Lidar and Infrared Pathfinder Satellite Observations (CALIPSO) platform are combined in the Synergized Optical Depth of Aerosol (SODA) algorithm and used to retrieve the optical depth of semitransparent single-layered cirrus clouds. In the operational CALIPSO data analysis, lidar-derived optical depths are typically estimated using a correction factor for multiple scattering effects and a single global mean lidar ratio. By combining the SODA approach with observations from the CALIPSO Imaging Infrared Radiometer, accurate values for both of these parameters can be derived directly from the measurements. Application of this approach yields a multiple scattering factor of 0.61 ± 0.15 sr, which is essentially identical to the value used operationally. However, the standard lidar ratio used in the CALIPSO daytime operational analysis is found to be biased low by around 25%. As a consequence, the lidar-derived optical depths retrieved from the daytime operational analyses are more than 30% smaller than those derived using SODA. The lidar ratio for semitransparent cirrus is found to be rather stable over ocean (33 ± 5 sr) with slight variations as a function of temperature and latitude. The geographic distribution shows a moderate decrease of average lidar ratio values over Indonesia during daytime, which may be attributed to a larger occurrence of high-altitude cirrus layers in this convectively active area.

Citation: Josset, D., J. Pelon, A. Garnier, Y. Hu, M. Vaughan, P.-W. Zhai, R. Kuehn, and P. Lucker (2012), Cirrus optical depth and lidar ratio retrieval from combined CALIPSO-CloudSat observations using ocean surface echo, *J. Geophys. Res.*, 117, D05207, doi:10.1029/2011JD016959.

1. Introduction

[2] The ice clouds effect on Earth's radiation budget is determined by the balance between the amount of solar radiation they absorb or reflect back to space, the amount of the terrestrial infrared radiation they absorb or reflect back to the surface, and their intrinsic thermal emissions. To first order, the quantities that determine whether this balance results in a net cooling or a net warming of climate are the ice clouds optical depths at visible and infrared wavelengths and their temperatures. The vertical information derived from the Cloud Aerosol Lidar with Orthogonal Polarization (CALIOP) on board the Cloud Aerosol Lidar and Infrared Pathfinder Satellite Observations (CALIPSO) [Winker *et al.*, 2010] is a significant step toward a better understanding of the ice cloud temperature, as it is directly linked to their altitude. However, determining the optical properties of

semitransparent ice clouds at visible wavelengths remains a challenging task.

[3] For passive sensors at visible wavelengths, the non-sphericity of ice crystals combined with the diversity of crystal sizes and shapes makes the retrieval of cirrus optical depth particularly challenging, as the accuracy of the determination is very sensitive to the ice crystals microphysical assumptions [Zhang *et al.*, 2009]. These same difficulties also apply to lidar profiling methods as lidar retrievals require the knowledge of the scattering phase function at 180° (i.e., the backscatter angle) and the contributions of multiple scattering in order to derive the optical depth from attenuated backscatter profiles. This can be done by taking advantage of combined lidar and infrared (IR) radiometry measurements using the so-called LIRAD method [Platt, 1973].

[4] In previous papers [Josset *et al.*, 2008, 2010a], we have developed a method using the collocated ocean surface return of CALIOP and of the CloudSat radar (the Cloud Profiling Radar, CPR) [Stephens *et al.*, 2008]. With this technique, we can retrieve the optical depth of semitransparent aerosol with no assumption about their microphysical properties, for daytime and nighttime measurements, and with a signal-to-noise ratio in the upper range of CALIOP capabilities. (The atmospheric features closest in term of

¹Science Systems and Applications, Inc., Hampton, Virginia, USA.

²LATMOS, IPSL, Université Paris VI, Paris, France.

³NASA Langley Research Center, Hampton, Virginia, USA.

⁴CIMSS, University of Wisconsin-Madison, Madison, Wisconsin, USA.

signal strength to the ocean surface are boundary layer water clouds, which have backscatter coefficients on the order of 10^{-2} to $1 \text{ km}^{-1} \text{ sr}^{-1}$, which is several orders of magnitude (up to around 3) higher than the typical backscatter coefficients of aerosols or cirrus clouds [Winker et al., 2009].) We show here that the Synergized Optical Depth of Aerosol (SODA) methodology can be extended to ice cloud optical properties retrievals, including lidar ratio (i.e., the ratio of the extinction coefficient to the backscatter coefficient), thereby offering a unified method to analyze the properties of aerosols and ice clouds in individual atmospheric columns. These improved estimates of lidar ratio should help reduce errors in extinction profile retrievals and lead to a better understanding of the climate radiation budget. Our methodology, called Synergized Optical Depth of Aerosol and Ice Clouds (SODA and ICE, shortened as SODA), is based on the fact that measurements made by the CloudSat radar are not attenuated by aerosols. CloudSat can then be used as a reference to retrieve the total attenuation of the CALIOP signals [Josset et al., 2008, 2010a] to further validate the operational products obtained in the frame of the CALIPSO mission [Winker et al., 2010].

[5] The general principles of the SODA technique are given in section 2, wherein we also review the additional error sources that are introduced when applying the method to ice clouds. Sections 3 and 4 describe those error sources in detail, focusing on marine aerosol contamination and multiple scattering effects and the methods we use to correct these errors. We then quantify the contribution of multiple scattering to the lidar signal by applying the LIRAD method to the combined measurements of CALIOP and the CALIPSO Imaging Infrared Radiometer (IIR) (A. Garnier et al., Retrieval of cloud properties using CALIPSO Imaging Infrared Radiometer. Part I: effective emissivity and optical depth, submitted to *Journal of Applied Meteorology and Climatology*, 2011). The overall uncertainties in our methodology are discussed in section 5. Results are shown in section 6, where we compare the SODA cirrus optical depth retrievals with the CALIPSO operational data products from both CALIOP and the IIR. Our retrieval of the lidar ratio of ice clouds is then presented and discussed in section 7, followed by the conclusion in section 8.

2. Formalism and Data Used in This Work

2.1. Generalities

[6] The very close collocation between CALIPSO and CloudSat observations within the A-Train (i.e., a temporal separation of 10 to 15 s and a perfect spatial collocation at the surface level) allowed us to develop an innovative method to analyze the lidar and radar ocean surface echo to retrieve the optical depth of aerosols [Josset et al., 2008, 2010a]. This approach is a new application of the spaceborne lidar and radar observations performed within the A-Train, and as such directly benefits from decades of research on ocean surface theory and ocean surface remote sensing analysis [Cox and Munk, 1954; Barrick, 1968; Valenzuela, 1970; Phillips, 1977; Valenzuela, 1978; Bufton et al., 1983; Jackson et al., 1992; Menzies et al., 1998; Liu et al., 2000; Li et al., 2005; Br  on and Henriot, 2006; Tanelli et al., 2008].

[7] CALIPSO and CloudSat ocean surface echo are linked together through interactions of electromagnetic waves with

the same rough surface area. Although system characteristics are different (and more particularly wavelengths and fields of views), a well-defined linear relationship can be identified locally between both scattering cross sections for most of the observational conditions [Josset et al., 2008, 2010a]:

$$\gamma_{SL,att} = f\left(\rho_{0L}, \frac{\sigma_{SR,att}}{\rho_{0R} T_{AR}^2}\right) T_{AL}^2 \approx F(\rho_{0L}, \rho_{0R}) \sigma_{SR,att} \frac{T_{AL}^2}{T_{AR}^2}, \quad (1)$$

where $\sigma_{SR,att}$ is the radar attenuated normalized surface scattering cross section (no unit, subscripts *S* for surface, *R* for radar, and *att* for attenuated). This quantity is called Sigma-Zero (σ_0) in the CloudSat operational product. We do not use decibel units in this study and σ_0 is linearized. $\gamma_{SL,att}$ (sr^{-1}) is the lidar integrated attenuated backscatter (subscript *L* for lidar) which is, for nadir pointing, the normalized scattering cross section [Barrick, 1968] at lidar wavelength divided by 4π [Bufton et al., 1983; Josset et al., 2010b]. ρ_{0R} and ρ_{0L} are the Fresnel reflectance coefficients at the radar and lidar wavelengths, respectively. The functions *f* and *F* express the link between all those quantities [Josset et al., 2010a]. T_{AR}^2 and T_{AL}^2 (subscript *A* for atmosphere) are the two-way atmospheric transmissions at the radar and lidar wavelengths, respectively. They are the total transmittances, including the contribution of any components present in the atmospheric column.

[8] Our goal is to retrieve the transmission of cirrus clouds at the lidar wavelength, T_{cirL}^2 (subscript *cir* for cirrus). Therefore, the correction of the attenuation by all other atmospheric component has to be established first. For the radar, the two-way atmospheric transmission, T_{mR}^2 (subscript *m* for molecules) includes the absorption by water vapor and oxygen. For the lidar (T_{mL}^2), it includes the attenuation by air molecules (nitrogen, oxygen) and absorption by ozone. The procedure to correct for those attenuations and the associated error analyses have been previously described [Josset et al., 2010a]. CloudSat water vapor attenuation is parameterized as a linear relationship of AMSR-E integrated water vapor path [Tanelli et al., 2008]. T_{AR}^2 and T_{AL}^2 also include an attenuation term due to aerosols at the lidar wavelength T_{aerL}^2 (subscript *aer* for aerosols) and due to cirrus clouds at the radar wavelength T_{cirR}^2 . We then have to determine the link between the single scattering attenuation by cirrus clouds, T_{cirL}^2 , and the measured attenuation of laser light which corresponds to the effective transmission, $T_{eff,cirL}^2$ (i.e., including multiple scattering contributions, subscript *eff* for effective). Doing this will require an analysis of multiple scattering effects, as several orders of scattering contribute to the measured lidar signal for ice clouds. For now, the effective atmospheric transmission as retrieved by SODA, can be written as

$$T_{AL}^2 = T_{mL}^2 T_{aerL}^2 T_{eff,cirL}^2, \quad (2)$$

$$T_{AR}^2 = T_{mR}^2 T_{cirR}^2. \quad (3)$$

By combining equations (1)–(3), the effective optical depth of cirrus clouds can be expressed as

$$\tau_{eff,cirL} = 0.5 \ln \left(F(\rho_{0L}, \rho_{0R}) \frac{\sigma_{SR,att}}{\gamma_{SL,att}} \frac{T_{aerL}^2 T_{mL}^2}{T_{mR}^2 T_{cirR}^2} \right). \quad (4)$$

Cirrus particles can be as large as several hundreds of micrometers in precipitating ice clouds [Heymsfield and Miloshevich, 2003] and can contribute to attenuation by scattering. The ice particle size is however smaller or comparable to the radar wavelength (3.2 mm). To estimate contributions from $T_{cir,R}^2$ we used the model of Ivanova *et al.* [2001] to parameterize ice crystal size distributions and Mie theory calculations [Bohren and Huffman, 1983], which provide the correct order of magnitude, even if particles of cirrus clouds are nonspherical. In any case, this approach slightly overestimates $T_{cir,R}^2$ as compared to a more realistic analysis for nonspherical particles [Mishchenko *et al.*, 2002]. CloudSat attenuation by absorption of the propagating beam in ice particles of cirrus clouds at 95 GHz can be totally neglected [Lhermitte, 1987]. Numerical simulations indicate that the relative error on $\tau_{eff,cirL}$ due to ice cloud radar attenuation $T_{cir,R}^2$ ranges between 0.04% to 0.35% for temperatures between -70°C and -30°C . As this correction remains very small, we will hereafter neglect it, considering $T_{cir,R}^2 = 1$ for the remainder of this study.

2.2. Formalism to Take Into Account Aerosol Contamination

[9] SODA retrieves the atmospheric attenuation of laser light by the total atmospheric column. Over the ocean, this column usually contains a mixture of boundary marine aerosols, variable amount of other types of aerosols transported from the continents (pollution, dust or biomass burning plumes, etc), and different types of clouds. If no correction for aerosols attenuation is applied, the quantity retrieved by SODA, $\tau_{tot,eff,L}$, is the sum of the effective cirrus and aerosol (τ_{aerL}) optical depths, as

$$\tau_{tot,eff,L} = \tau_{eff,cirL} + \tau_{aerL} = 0.5 \ln \left(F(\rho_{0L}, \rho_{0R}) \frac{\sigma_{SR,att}}{\gamma_{SL,att}} \frac{T_{mL}^2}{T_{mR}^2} \right). \quad (5)$$

The CALIPSO operational products (CALIOP level 2 Aerosol layer or IIR level 2) can be used to find observations with no aerosol layer detected. However, even if we apply this criterion some weak or diffuse features mainly coming from marine boundary layer aerosols may be undetected and thus still be present in our retrieval at a level of a few percent. This will introduce an overestimation of the optical depth and a positive bias on average that needs to be corrected, as will be discussed in section 3.

2.3. Formalism to Take Into Account Multiple Scattering and Infrared Observations

[10] Ice and water clouds can induce a noticeable amount of multiple scattering in lidar return [Eloranta, 1998]. Different formalisms with different levels of complexity can be used to take into account lidar multiple scattering [Platt, 1973; Eloranta, 1998; Bissonnette, 1996]. In presence of multiple scattering, the effective cirrus optical depths retrieved by a lidar system are lower than the single scattering optical depth, as the different orders of scattering can stay within the field of view and photons continue to be detected. A simple way to account for multiple scattering in the lidar equation was proposed by Platt [1973], who introduced the reduction factor η relating the cloud optical

depth, $\tau_{cir,L}$, to the effective optical depth, $\tau_{eff,cirL}$, so that $\tau_{eff,cirL} = \eta \tau_{cirL}$.

[11] The determination of the optical depth thus requires the determination of the multiple scattering factor η . Platt [1973] and subsequent authors used thermal IR radiometric data to infer cloud optical depth and retrieve lidar parameters. Here, we will follow his approach by using the CALIPSO IIR “track” observations which are by design spatially and temporally collocated with the CALIOP profile measurements. The cirrus absorption optical depth (CAOD), $\tau_{abs,IR}$, in the IR is linked to the absorption emissivity $\varepsilon_{abs,IR}$ as

$$\tau_{abs,IR} = -\ln(1 - \varepsilon_{abs,IR}). \quad (6)$$

For large particle sizes, the exact limit of extinction to absorption efficiency, Q_{ext} and Q_{abs} , in the infrared can be derived from geometric optics, so that

$$\frac{1}{A_D} = \frac{Q_{ext}}{Q_{abs}} = \frac{2}{1 - Q_{refl}} > 2. \quad (7)$$

In equation (7), A_D is the ratio of the absorption to extinction optical depth in the infrared; Q_{refl} is the amount of light reflected by the ice crystal. Its determination requires an exact knowledge of the ice crystal shape, orientation, light incident direction and polarization state. To give a sense of the order of magnitude, Q_{refl} is around 2% for a planar surface and around 7% for a large sphere [Bohren and Huffman, 1983]. It should be noticed that although this ratio $1/A_D$ is close to 2 for large particles it can tend to 1 when absorption is important (imaginary part of the refractive index on the order of 0.1) and the size parameter much lower than unity. We further introduce the ratio B of visible (obtained at the lidar wavelength) to IR optical depth. For spheres with large size parameter, $B \sim 1$.

[12] From measurements, we do not access the IR CAOD, but a proxy derived from the natural logarithm of the effective coemissivity $1 - \varepsilon_{eff,IR}$ in a way similar to equation (6). Introducing the ratio of the IR CAOD to its proxy as C_e , we can thus write for cirrus clouds,

$$\tau_{cir,L} = -B \cdot A_D \cdot C_e \ln(1 - \varepsilon_{eff,IR}). \quad (8)$$

As shown by Platt [1973], the integrated lidar signal can be written in his integrated form as

$$IAB = \frac{1 - e^{-2\eta\tau_{cirL}}}{2\eta S}. \quad (9)$$

Equation (9) links the integrated attenuated backscatter signal (IAB in sr^{-1}) to the multiple scattering coefficient η , the true optical depth τ_{cirL} and the lidar ratio S (sr), defined as the ratio of cloud extinction to backscatter coefficients, or the inverse of the normalized phase function at 180° (assuming a single scattering albedo equal to 1 at 532 nm). All quantities in equation (9) refer to light scattering by ice crystals particles only. The subscript *cir* has not been added in the definition of the multiple scattering coefficient and lidar ratio as there is no ambiguity possible in this study. In our approach, the effective optical depth $\eta\tau_{cirL}$ is the value we directly retrieve (that is $\tau_{eff,cirL} = \eta\tau_{cirL}$).

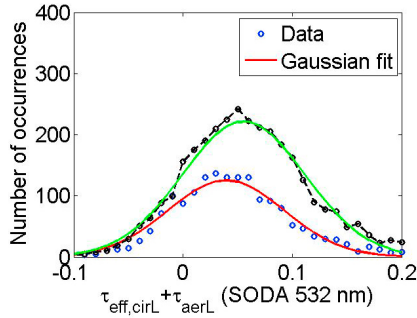


Figure 1. Distribution of the total column optical depth (including aerosols and cirrus) at 532 nm retrieved by SODA for the lowest IIR emissivities. The circles are for IIR emissivities of 0.01 ± 0.005 , and the dashed line is for IIR emissivities of 0.02 ± 0.005 . The Gaussian best fit to the data is superimposed for both cases (solid lines). The analysis is applied to 1 year of daytime data (2010) and to single-layer cirrus clouds with no detected aerosols (IIR scene type 21).

[13] One can then combine equations (5) and (8) to link the lidar optical depth derived from SODA and the IR emissivity from the IIR measurements and thus obtain the relationship linking the cloud optical depth as retrieved from ocean surface and the infrared emissivity. From this relationship, we derive the multiple scattering factor,

$$\eta = -\frac{\tau_{\text{tot eff},L} - \tau_{\text{aer},L}}{B_{AD}C_e \ln(1 - \varepsilon_{\text{eff},IR})}, \quad (10)$$

which once determined will enable subsequent retrievals of the desired (i.e., single-scattering) atmospheric parameters.

2.4. Data Used in This Work

[14] The SODA algorithm based on the work of Josset *et al.* [2010a] has been applied to 1 year (2010) of CALIPSO level 1 version 3 data and CloudSat level 1 version R04 data as well as the corresponding AMSR-E daily ocean product. The data are produced and archived at the French thematic center ICARE (Cloud-Aerosol-Water-Radiation Interactions). The IIR level 2 version 3 track product (IIR_L2) and CALIOP level 2 version 3 5 km cloud layer products (CAL_05kmCLay) are also used in this study. For passive instruments, the comparison is performed with the closest pixel from the CAL_05kmCLay grid point at the surface level. The data used in this study are restricted to single-layer semitransparent cirrus clouds without aerosols detected in the atmospheric column (based on the CALIPSO level 2 cloud and aerosol layer products). This corresponds to IIR scene type 21 (Garnier *et al.*, submitted manuscript, 2011). Furthermore, unless otherwise specified, the only layers included in this study are those identified as ice with high confidence by the CALIOP ice-water phase algorithm [Hu *et al.*, 2009] and for which the full IIR microphysical retrieval could be performed. Finally, the midcloud temperature as reported in IIR_L2 (centroid temperature (Garnier *et al.*, submitted manuscript, 2011)) has been limited in the -70°C to -40°C range to reduce possible contamination of the data set by supercooled liquid water clouds or by polar stratospheric clouds. The analysis is focused on the 532 nm channel only. Note that the data have been filtered this way

because the properties of the geophysical feature analyzed (single-layer semitransparent ice cloud over the ocean with no aerosols below) are retrieved with reasonably high confidence by the active and the passive instruments and there is no ambiguity in the domain of validity of the algorithms. The results are not expected to change significantly by extending the temperature range or by considering multilayer clouds. Opaque clouds or multilayer cloud/aerosol features would require in-depth analyses.

[15] To facilitate comparisons with previous studies using space-based observations by passive sensors in the visible spectral domain, most of the results shown here are derived from daytime data only. The signal-to-noise ratio of CALIOP ocean surface return is higher than for most atmospheric measurements and thus the quality of SODA products remains high for both daytime and nighttime. Although, the CALIOP calibration is expected to be of lower quality during daytime [Powell *et al.*, 2010], we have checked that using nighttime data would not change our conclusions.

3. Determination of Marine Aerosol Baseline From CALIPSO IIR Observations

[16] As discussed previously, our analysis is applied to single-layer semitransparent high clouds over the ocean with no aerosols layer below. However, some undetected marine boundary layer aerosols could actually be present, as their low altitude combined with their low optical thickness can make them difficult to discriminate from clear air layers. This does not affect IIR observations but will create a small bias in SODA which has to be corrected. Dust aerosols uplifted in the upper troposphere may be imbedded in cirrus clouds [Huang *et al.*, 2006] and not detected by CALIOP. This would cause the IIR retrieval to fail and results not to be included in the analysis as the spectral behavior is mixed between dust and clouds which would prevent to retrieve coherent values of the cloud particle size using the two wavelength pairs (Garnier *et al.*, submitted manuscript, 2011). The optical depth determined from the emissivity in the infrared using equation (8) is thus entirely due to cirrus cloud. It will converge to 0 with decreasing emissivity. However, according to equation (5), $\tau_{\text{tot eff},L}$ will converge to the aerosol optical depth. Using equations (5) and (8), we can thus retrieve the statistical properties of the aerosol contamination as the asymptotic value for decreasing emissivity for colocated CALIOP, CloudSat and IIR observations represented by the variations of $\tau_{\text{tot eff},L}$ as a function of infrared emissivity.

[17] Figure 1 shows the optical depth derived from SODA at 532 nm for the lowest cirrus infrared emissivities as observed by the IIR at $12 \mu\text{m}$. We have considered SODA total optical depths for low values of IIR emissivities of 0.01 ± 0.005 and 0.02 ± 0.005 . Those distributions are shown in Figure 1. The mean SODA optical depths for the two IIR emissivity ranges are 0.04 and 0.06, respectively. An uncertainty of around ± 0.05 is associated with those two values.

[18] As expected from equation (8), the mean optical depth retrieved by SODA converges to a value close to 0 as the magnitudes of the emissivities considered approaches 0. This behavior allows us to determine the slope of the

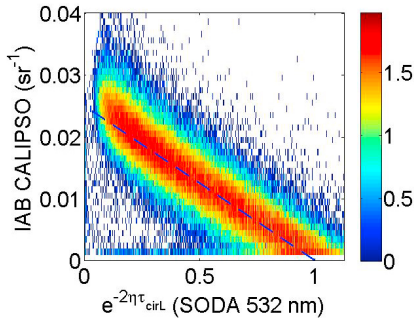


Figure 2. CALIPSO integrated attenuated backscatter coefficient (IAB) at 532 nm as a function of SODA optical depth after correction for the small bias due to undetected aerosols. The dashed line gives the best linear fit with a transmission of 1 when IAB is equal to 0. The color is the logarithm of the number of observations. The analysis is applied to 1 year of daytime data (2010) and to single-layer cirrus clouds with no aerosols detected (IIR scene type 21).

relationship between visible and infrared optical depth which is equal to BA_D . This will be discussed in section 4.

[19] We find by linear extrapolation that the SODA optical depth converges to a value of τ_{aerL} equal to 0.02 ± 0.05 when the IIR emissivity tends to zero. This value of the positive bias will be used in the following to determine τ_{cirL} . The positive bias (0.02) can be considered as a systematic error linked to marine boundary layer aerosols which can be corrected by a simple subtraction.

[20] The standard deviation (0.05) is a good estimation of the error bar in the observations we are using. It includes all error sources: instrumental noise, correction of molecular attenuation at lidar and radar wavelength, accuracy of lidar and radar calibration and natural variability of the aerosol optical depth in the marine boundary layer. We will thus consider an error estimation in our retrieval is $\Delta\tau_{eff,cirL} = 0.05$. It is the error associated with a straightforward use of SODA combined with the current version 3 IIR_L2 and CAL_05kmCLay products. It may be possible to reduce this error in the future as those different products will evolve but, as we will see, this level of accuracy already allows us to obtain and discuss interesting results.

4. Lidar Parameter Analysis

4.1. Effective Lidar Ratio

[21] Figure 2 shows CALIOP integrated attenuation backscatter coefficient (IAB) from CAL_05kmCLay for the whole year of 2010 as a function of the measured two-way cirrus transmission ($\Xi = e^{-2\eta\tau_{cirL}}$) determined from SODA data analysis using the surface return and after correcting for the background aerosol transmission, as identified in section 3. As expected from equation (9), IAB is seen to be well expressed as a linear relationship of the two-way cirrus transmission. We also analyzed data for January 2007 and 2008 and obtained identical relationships between the two measurements. The dispersion of the points is due to the noise in the data and to atmospheric variability. The noise induces a dispersion comparable to results plotted in Figure 1 derived for $IAB \sim 0$. Atmospheric variability is expected to increase the (relative) error as the transmission

decreases. The good agreement between data and basic lidar theory strongly points to a remarkable statistical stability of the product ηS as a function of optical thickness.

[22] The data as presented here do not exclude a slight deviation at effective optical thickness larger than 0.8 (effective two-way transmission smaller than 0.2), as seen in Figure 2 for the departure of the fitted line. Using the best fit to the two-way transmission data, and forcing the transmission for clear atmosphere to be equal to 1, we find the average effective lidar ratio $\eta S = \frac{1}{2IAB_0}$, to be 20 sr with the value at zero transmission equal to $IAB_0 = 0.025 \text{ sr}^{-1}$. Extreme values (one standard deviation away from the median) would range from 0.022 to 0.029 sr^{-1} (e.g., ηS ranging from around 23 to 17 sr). One can notice that the trend for low transmission data would lead to values in the upper range of IAB and lower range of ηS . It is to be noticed that the fixed value of ηS used to retrieve most of the daytime cirrus optical depths reported in CAL_05kmCLay is equal to 15 sr, which is 25% lower than what the average value of 20 sr we find here. Using this low value has several consequences which will be examined in details in section 6.

[23] A previous study analyzing CALIPSO version 2 data for 2008 in dense cirrus [Baum *et al.*, 2010] lead to similar values of ηS . Most of the data of Baum *et al.* [2010] fall in the range $IAB = 0.024\text{--}0.032 \text{ sr}^{-1}$ (ηS from 16 to 21 sr) when $e^{-2\eta\tau} \sim 0$. The slightly higher IAB values may be consistent with the deviation we observe at high optical thickness and we will come back to this point in the discussion. In order to understand this behavior and determine the single scattering optical depth, we further need to determine the contribution of multiple scattering.

4.2. Multiple Scattering Coefficient Analysis

[24] The analysis using infrared emissivity as previously introduced provides guidance in determining the value of the multiple scattering factor using equation (10). From the ratio of SODA optical depth to IIR optical depth as expressed by equation (10) we can derive the average value of ηBA_D , which can then be compared to the estimates of the mean effective diameter for ice clouds provided in the IIR_L2 product. Considering various nonspherical particle shapes, it has been shown (Garnier *et al.*, submitted manuscript, 2011) that the effective absorption optical depth determined from measured radiances using effective emissivity $\epsilon_{abs,IIR}$ at $12 \mu\text{m}$, is a good proxy for absorption optical depth, as scattering in clouds remains low at this wavelength. The ratio C_e is equal to 1 (within a few percent) on average, and varying by less than 10% with OD, size and shape (Garnier *et al.*, submitted manuscript, 2011). We will further consider $C_e = 1$, as we will focus on a statistical analysis.

[25] Using the high confidence global observations of SODA and the IIR, taking into account quality indices, we determined the distribution of ηBA_D as a function of particle size derived for all emissivity values and temperatures colder than -40°C (thus ensuring that we considered only ice clouds) and excluding the few data with temperature lower than -70°C . To minimize the effects of aerosol contamination, data for which the SODA optical depths were smaller than 0.25 were removed from the analysis. Applying this

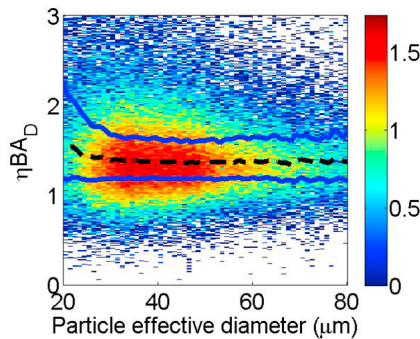


Figure 3. The parameter ηBA_D as a function of particle size for ice clouds ($-70^\circ\text{C} < T < -40^\circ\text{C}$), color-coded according to the logarithm of the number of observations for 1 year of daytime data (2010) for single-layer cirrus (IIR scene type 21). The black dashed line shows the median of the data, and the two solid blue lines are the first and third quartiles.

filter simultaneously minimizes retrieval errors in the IIR effective diameter (IIR_L2 product). Optical depth values larger than 3 are not present. Figure 3 shows the variations of the quantity ηBA_D as a function of particle effective diameter.

[26] The median value of the data shown in Figure 3 increases slightly for diameters smaller than $30\ \mu\text{m}$. The effective diameters reported in IIR_L2 products are derived using a split-window approach to determine by pairs the ratios of the IIR effective optical depths retrieved at 8.65, 10.6 and $12.05\ \mu\text{m}$. At first order, this retrieval is not a function of the $12\ \mu\text{m}$ optical depth but of its ratio to the values retrieved in the two other channels. This combined with the fact that the SODA optical depth and the IIR optical depths at 8.65 and $10.6\ \mu\text{m}$ are totally independent variables should ensure that ηBA_D and the effective particle diameter are independent. This is different from a simultaneous retrieval of cloud visible optical depth and particle size as is done in current passive remote sensing algorithms [Platnick *et al.*, 2003]. The median value of the particle diameter coming from IIR observations and as reported in Figure 3 is equal to $41\ \mu\text{m}$.

[27] For this particle diameter, the median value of ηBA_D is equal to 1.37 ± 0.3 , which correspond to the standard deviation of a normal distribution which would have the same dispersion between the median and the first and third quartiles. Owing to the shape of the curve, errors on particle size will not have a major impact on the determination of the multiple scattering factor. However, it is directly depending on the value of BA_D chosen. Several authors have reported values for the BA_D product [Minnis *et al.*, 1993; Fu and Liou, 1993; Platt *et al.*, 2002]. We will refer here to the theoretical value of BA_D reported by Platt *et al.* [2002, hereinafter PL02] from calculations made for several shapes by Mitchell *et al.* [1996], wherein BA_D is seen to be weakly increasing from 2.1 to 2.3 as particle diameter decreases from 70 to $30\ \mu\text{m}$. Previous observations using LIRAD method support these values [Platt *et al.*, 1998; Sassen and Comstock, 2001], as well as other calculations [Fu and Liou, 1993]. This means values of the multiple scattering factor would vary between 0.65 and 0.59. It would not be

much larger for very small particles as ηBA_D is then increasing. Considering $20\ \mu\text{m}$ diameter particles, one would derive $\eta \sim 0.61$. As a result, one should consider that the value of 0.61 proposed applies to all particle sizes and not only to the median value. No impact is expected even if error in particle size is considered in this range. A ratio of the results from Figure 3, C_e dispersion and PL02 results leads to a constant value of $\eta = 0.61 \pm 0.15$ for the observations of SODA and IIR and the dispersion referring to all individual measurements. When the average value and identified shapes are considered the dispersion is much smaller.

[28] Although this is close to the value of the multiple scattering factor considered up to now in the CALIOP operational algorithm (0.6 [Young and Vaughan, 2009]) based on comparison with the Cloud Profiling Lidar, it is not totally consistent with Monte Carlo analysis [Winker, 2003] showing phase function dependency of the multiple scattering factor (varying from around 0.6 to around 0.8) or recent advances in lidar multiple scattering analytical approach [Hogan, 2008] which are at the upper and lower part of the uncertainty range, respectively. IIR optical depth values may be biased low owing to limitations in sensitivity in the IR analysis method as cloud optical depth increases. This would bias the multiple scattering factor we retrieve toward higher values, but this is expected to only occur for denser clouds, when the visible optical depth exceeds 3 as IR retrieval saturates, owing to the limited absorption sensitivity. We will reevaluate this value in the future as further advancements are made in infrared radiative transfer and with each significant evolution of IIR, CALIOP and SODA retrieval algorithms.

[29] The LIRAD approach has also been used by Lamquin *et al.* [2008] to determine CALIPSO multiple scattering using a combination of the infrared sounder AIRS and CALIPSO Version 1 data using direct transmission method, and assuming $BA_D = 2$. Their analysis led to a multiple scattering factor varying between 0.45 and 0.55 for the coldest clouds as a function of emissivity. The values of BA_D considered here are about 10% higher, which would lead to an equivalent reduction in the multiple scattering values. There are therefore important differences with our results that cannot be explained by using different values of BA_D . It should be noted that the collocation and comparison of the visible and IR measurements are more difficult since two satellites from the A-Train (CALIPSO and AQUA) were considered and AIRS IR pixels are larger ($13.5\ \text{km}$ at nadir [Yue and Liou, 2009]) compared to the IIR pixels. The determination of the “direct transmission” optical depth using CALIPSO version 1 data and the methodology used by Lamquin *et al.* [2008] is a complex process. It requires extremely accurate detection of cloud boundaries and determination of what is clear air or cloudy air. Contrary to CALIOP operational product (CAL_05kmCLay), it is affected by instrument calibration as only molecular signal from below the cloud is used. Furthermore, the analysis was limited to tropical area where CALIOP calibration can be affected by stratospheric aerosols [Vernier *et al.*, 2009, 2011]. The large size of AIRS pixel combined with the low statistics of high-quality potential candidates for “direct transmission” may cause problems in the subsequent analysis of the data.

[30] As previously mentioned, the multiple scattering factor we find is different from the one derived from analytical calculations [Eloranta, 1998; Hogan, 2008]. For nonabsorbing particles, half of the scattered energy is contained within the small angle of the forward diffraction peak. The small-angle multiple scattering regime applies when only the scattered energy contained within the forward peak contributes to the detected multiple scattering. This defines a lower limit of $\eta = 0.5$ [Eloranta, 1998], but larger values can be obtained if the diffraction peak does not remain in the detection cone. Going to large optical depths leads to increased horizontal transport of light, which causes η to become smaller than the small angle limit, as in this case light scattered within large angle can contribute to the multiple scattering by being reinjected inside the lidar field of view [Chepfer et al., 1999]. The limitation between small-angle multiple scattering regime and wide-angle multiple scattering [Hogan, 2008] happens when the width of the projected area of the field of view, D (m), becomes comparable to the scattering mean free path l . As absorption by ice particles can be neglected at CALIOP wavelength (532 nm and 1064 nm, with only the first one being considered in this study), the scattering mean free path l_t (m) is

$$l_t = \frac{1}{\alpha_s(1-g)}. \quad (11)$$

In equation (11), α_s (m^{-1}) is the cloud scattering coefficient and g is the asymmetry factor. The (upper range) extinction limit requirement for small angle multiple scattering is defined by

$$D \ll l_t. \quad (12)$$

The asymmetry factor g for cirrus clouds is estimated to be in the 0.77–0.89 range [Labonnote et al., 2000; Yang et al., 2008a, 2008b] so that $(1-g)$ will be between 0.11 and 0.23. For CALIOP the projected size of the telescope field of view D is around 90 m so the extinction has to be much lower than 0.048 m^{-1} considering the smallest value. This corresponds to an optical depth of about 50 for a 1 km thick cloud and the requirements for small-angle multiple scattering will be fulfilled all the time when an ocean surface echo is observed. We are therefore well in the domain of application of the analytical calculations.

5. Uncertainty Analysis

5.1. Optical Depth Uncertainty

[31] Errors in standard SODA analysis have already been discussed in previous publications [Josset et al., 2008, 2010a]. The SODA methodology can be applied to the retrieval of cirrus cloud optical depth the same way it is done for aerosols, but the associated uncertainty estimates must also account for additional error sources related to the determination of multiple scattering, and the residual error on the contribution of undetected layers below the cirrus layer.

[32] We are here following the standard definition of the uncertainty [Joint Committee for Guides in Metrology, 2008]. The total uncertainty (square root of the variance) Δy on a parameter y which can be expressed as a function

$y = f(x_1, x_2, \dots, x_N)$ of a number N of other measured input parameters x_1, x_2, \dots, x_N can be written as

$$\Delta y = \sqrt{\sum_{i=1}^N \left(\frac{\partial f}{\partial x_i} \right)^2 (\Delta x_i)^2 + 2 \sum_{i=1}^{N-1} \sum_{j=i+1}^N \frac{\partial f}{\partial x_i} \Delta x_i \frac{\partial f}{\partial x_j} \Delta x_j r(x_i, x_j)}, \quad (13)$$

where i and j represent the index on which the summations are done and $r(x_i, x_j)$ is the correlation coefficient between the measured parameters x_i and x_j . In our study, the measured input parameters are the effective optical depth ($\tau_{\text{eff}, \text{cirL}}$), the multiple scattering coefficient η and the integrated attenuated backscatter (IAB). The correlation between the different measurements have been neglected as they are estimated independently through a combination of different instruments and η do not show pronounced variation as a function of the effective optical depth (Figure 2).

[33] Taking into account multiple scattering effects, the first-order error on the cirrus optical thickness can be written as

$$\Delta \tau_{\text{cirL}} = \sqrt{\left(\frac{\Delta \tau_{\text{eff}, \text{cirL}}}{\eta} \right)^2 + \left(\frac{\Delta \eta}{\eta} \tau_{\text{cirL}} \right)^2}. \quad (14)$$

As we have previously discussed, 0.05 is a good estimate of the effective optical depth error and includes all error sources. The error on the estimation of the multiple scattering factor $\Delta \eta$ will linearly impact the accuracy of the retrieved optical depth. Following our previous analysis, a value of $\eta = 0.6$ has been used in the following.

[34] Our error bar (absolute error) on cirrus optical depth is thus $\Delta \tau_{\text{cirL}} = \sqrt{(0.08)^2 + (0.25 \tau_{\text{cirL}})^2}$. We expect to reduce this number in the future by a better correction of the low-level aerosol contribution and further refinement of CALIOP multiple scattering correction. The multiple scattering code of Hogan [2008] points to a stability of CALIOP multiple scattering on the order of 3% for ice particles which is much smaller value than the uncertainty of 25% we have here. We cannot reduce this value until we have solved the discrepancy between our observations and lidar multiple scattering theory but this result combined with the high stability observed in Figure 2 could suggest that in the future, we will be able to derive a value with an error bar much lower than the 25% currently associated with this parameter.

5.2. Lidar Ratio Uncertainty

[35] The relative error on the lidar ratio can be derived from equations (9) and (13) as a function of the error on the cirrus effective optical depth $\Delta \tau_{\text{eff}, \text{cirL}}$, on the particle column integrated attenuated backscatter ΔIAB (sr^{-1}) and on the multiple scattering coefficient $\Delta \eta$:

$$\frac{\Delta S}{S} = \sqrt{\left(\frac{2 \Delta \tau_{\text{eff}, \text{cirL}}}{e^{2 \tau_{\text{eff}, \text{cirL}}} - 1} \right)^2 + \left(\frac{\Delta \text{IAB}}{\text{IAB}} \right)^2 + \left(\frac{\Delta \eta}{\eta} \right)^2}. \quad (15)$$

The first term of equation (15) expresses the relative error on the effective optical depth. The second and third terms express the relative error on the IAB and η both present in

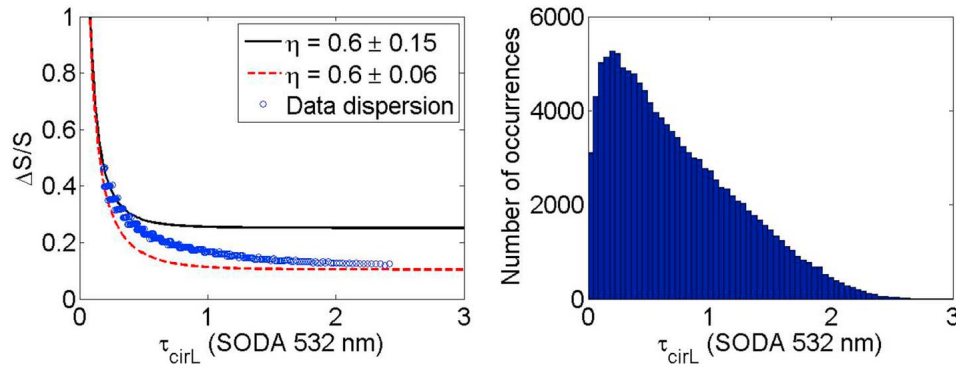


Figure 4. (left) Expected relative error of the cirrus lidar ratio retrieval as a function of cirrus optical depth (solid line) coming from our derivation. For reference, a smaller relative error on multiple scattering factor (dashed line) and the data dispersion (circles) of Figure 2 ($\Delta IAB/IAB$; see text) are represented. (right) Histogram of the cirrus optical depth analyzed in this study.

the denominator of the right term of equation (9). If we take into account a relative error of 3% in IAB due to calibration [Rogers *et al.*, 2011], and the error on optical depth derived in section 5.1, the relative error on lidar ratio is mainly due to the relative error on the multiple scattering factor. The resulting relative error is shown in Figure 4.

[36] It has to be acknowledged that our lidar ratio error estimates depend on the uncertainty in the derivation of the multiple scattering factor determined by applying the LIRAD method to CALIOP and IIR data (0.61 ± 0.15 sr), and that the multiple scattering uncertainty includes dispersion due to the optical depths in the visible and IR, as well as the variation of their ratio with cloud properties. We further note that the estimated total uncertainty appears to be larger than the intrinsic variations of the multiple scattering factor observed in the data reported in Figure 2. We do not have enough elements at the time of this study to derive precisely around which value this error bar should be reduced. For reference, the relative dispersion of the data as observed in Figure 2, which is $\Delta IAB/IAB$ (the ratio of the standard deviation of the data on the median value), is shown in Figure 4. The error budget for $\Delta IAB/IAB$ is similar to $\Delta S/S$ and those two terms can be inverted in equation (15) if a calibration error term is added on the right part of equation (15). The uncertainty on IAB is higher than on the lidar ratio as geophysical variations of the lidar ratio are expected (i.e., $\Delta S/S$ is unlikely to be 0 for a given IAB), and this may explain why the data dispersion do not correspond perfectly to the standard uncertainty. As we can see, the data dispersion (circles) in Figure 4 is much lower than what would be obtained assuming a larger error bar corresponding to our identified uncertainty (solid line). The absolute value and mean variation observed are more directly seen to be in better agreement with the error bar in the lidar ratio derived assuming the multiple scattering factor is stable and seems to converge toward a value expressed by 0.6 ± 0.06 sr (Figure 4, dashed line), and this is consistent with a limited variation of the multiple scattering factor. In other words, the natural variability of the ice crystal phase functions, appears to have a limited impact on the variations of the CALIOP multiple scattering factor. This stability and limiting the analysis to a relatively high number of observations to lower the dispersion will

allow us to make preliminary but meaningful discussion of the lidar ratio. The uncertainty as discussed in this section corresponds to a standard deviation associated with the individual retrievals. This means the uncertainty should decrease approximately as the square root of the number of observations. For 100 observations, a relative uncertainty of 10% should reduce to around 1%.

6. Cirrus Optical Depth Retrieval: Comparison With Operational CALIPSO Products

[37] CALIOP operational product (CAL_05kmCLay) uses two different approaches to retrieve cloud extinction and optical depth [Young and Vaughan, 2009]. The most often used technique, called hereinafter “inversion,” retrieves optical parameters by solving the lidar equation (also called Fernald-Klett equation, from the names of the first analyses made by Fernald *et al.* [1972] and Klett [1981]) assuming a fixed lidar ratio of 25 sr and a multiple scattering factor of 0.6. The more accurate approach, which we will call the “direct transmission,” is used whenever a layer of clear air (i.e., molecular air with as few aerosols as possible) is present both immediately over and immediately below the cloud layer. In these cases, the optical depth of the layer can be retrieved directly, with the only errors being due to the estimation of clear air backscatter coefficient and uncertainties in the value of the multiple scattering [Young, 1995; Young and Vaughan, 2009]. The “direct transmission” approach is mostly applicable during nighttime as the CALIOP signal-to-noise ratio is substantially higher and detection of clear air also more accurate. A very limited number of retrievals are performed this way during daytime.

[38] Figure 5 shows a comparison of the total column optical depth obtained from the CALIOP operational product (CAL_05kmCLay) as a function of the optical depth measured by SODA for 1 year (2010) of nighttime data. Only those data corresponding to single-layer cirrus with optical depths measured using the “direct transmission” method (e.g., no assumption on lidar ratio) are used. SODA and CALIOP error sources have already been discussed in detail in previous papers. For CAL_05kmCLay, the error comes from the accuracy of the molecular scattering profile used in the retrieval and the amount of aerosol over and

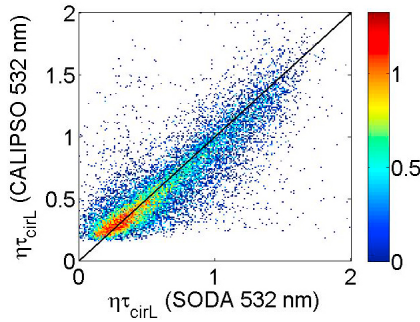


Figure 5. CALIPSO retrievals using the “direct transmission” approach as a function of SODA for 1 year (2010) of nighttime data. The data are restricted to constrained retrievals for which no other layers were detected in the profile. We can see an extremely good agreement between the two retrieval methods with most of the data scattered around the 1:1 line.

below the cloud. As we are comparing a total column retrieval (SODA) with a range resolved – or at least layer by layer – retrieval (CAL_05kmCLay), any undetected features below the cloud could still partially affect SODA even after the global bias has been corrected as described in section 3. Overall, Figure 5 shows an extremely good agreement between the effective optical depth of cirrus and SODA as most of the data are scattered close to the 1:1 line.

[39] Going back to daytime data, Figure 6 shows the comparisons between SODA, IIR (IIR_L2), and CALIOP (CAL_05kmCLay) single-layer cloud total optical depth for 2010 (daytime). As there is a very limited number of daytime CALIOP using the “direct transmission” method, Figure 6 can be considered as a comparison of SODA with the CALIOP “inversion” technique. There is a good agreement (correlation of 0.89) between IIR and SODA, and the slope of 0.43 (i.e., close to the inverse of 2.25) comes from the relation between visible extinction and IR absorption, we find consistently with our initial hypothesis, after the multiple scattering correction has been applied. The high correlation (0.81) with the CALIOP operational product (Figure 6, right) is not surprising considering the link

between IAB and transmission retrieval from ocean surface as shown in Figure 2. The difference with SODA comes from a difference in the effective lidar ratio, as the CALIOP operational inversion algorithm assumes a value of the effective lidar ratio equal to 15 sr. As we can see in Figure 6, the data are mostly below the 1:1 line. The difference in effective lidar ratio is around 25% with the value we derived from data shown in Figure 2, but owing to the nonlinearity of the Fernald-Klett equation, the difference increases as optical depth increases. For the comparison of SODA and CALIOP as given in Figure 6, the slope of the best fit (constrained to go through 0) using data with optical depth lower than 0.5 is around 2/3 which corresponds to a difference of around 33% which is shown by the dashed line in Figure 6 (right). Because of the nonlinearity of the retrieval, this slope decreases (which appears like a “saturation effect”) at high optical depth, as we can see if we fit the data with a second-order polynomial curve (the dash-dotted line in Figure 6, right). This corresponds to a difference of around 41% for an optical depth of 2.

[40] More simply stated, the good agreement between SODA and CALIOP for the “direct transmission” algorithm but not for the “inversion” algorithm indicates that the value of the lidar ratio chosen for the “inversion” algorithm is too low.

7. Lidar Ratio Analysis

7.1. Results Presentation

[41] Using SODA, we can determine the lidar ratios S of ice clouds and begin to investigate their geographical distribution. For nonabsorbing particles, the lidar ratio is the inverse of the phase function at backscatter angle [Holz, 2002; Baum *et al.*, 2010] (usually normalized by a factor 4π) and can thus provide an information to better determine the ice crystals phase function [Labonnote *et al.*, 2000; Xie *et al.*, 2009; Yang *et al.*, 2008a] and improve microphysical models used in passive retrievals [Baum *et al.*, 2005, 2011]. In this section, we excluded cirrus optical depths smaller than 0.25 from the data analysis, so as to minimize errors arising from aerosol contamination in the region below the clouds and errors in S values (see Figure 4).

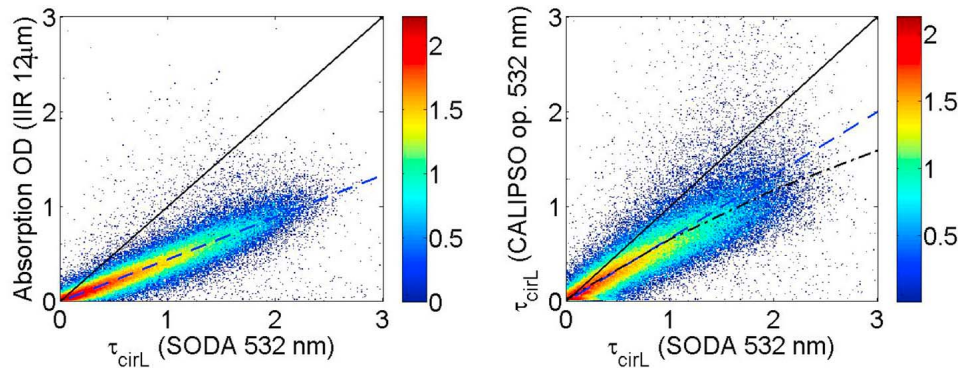


Figure 6. (left) Absorption optical depth as retrieved by the IIR as a function of SODA for daytime. The dashed line is the 2.25:1 slope. (right) Optical depth as retrieved by the CALIOP operational product as a function of SODA. Color represents the logarithm of the number of observations in each bin. The black solid line is the 1:1 line. The dashed line is the 3:2 slope as fitted for low optical depths. The dash-dotted line is the second-order polynomial best fit.

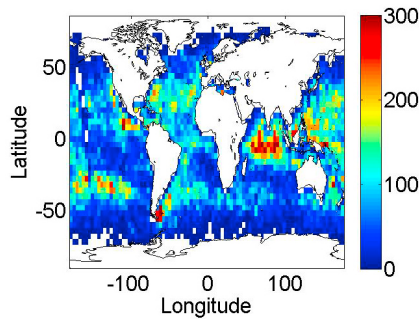


Figure 7. Map of the number of observations in a 4 degree by 4 degree pixel where single-layer cirrus without aerosols below it (IIR scene type 21) was detected for 1 year of day-time data (2010).

[42] Figure 7 shows the number of observations in a 4 degree by 4 degree pixel when using the criteria used to create Figure 2. The observations are relatively well distributed but there are fewer observations toward the poles and the southern midlatitude. Because of the aerosol statistical correction procedure we employed, areas with low numbers of data points may contain a residual positive bias due to undetected aerosols. For this reason, the lidar ratio map shown in Figure 8 is restricted to the pixels containing more than 100 observations, and we limit our discussion to the variations of large clusters of pixels.

[43] According to the previous discussions, from Figure 2 we can derive a mean lidar ratio above oceans equal to 33 ± 5 sr. If we exclude the latitudinal area beyond 50°S and 50°N , which do not contain a lot of observations, we can see in Figure 8 a minimum value at low latitude (around 31 sr at 5°S) and a slight increase toward midlatitudes (around 34 and 36 sr in the midlatitude storm track areas at 40°N and 40°S , respectively). This may be linked to regional differences possibly induced by dynamical and radiative forcings as lower values are mostly observed over Indonesia in deep convection areas.

[44] Figure 9 (left) shows the lidar ratio as retrieved as a function of the midcloud temperature and a map of the cloud temperature (Figure 9, right). The median lidar ratio is shown to vary between around 31 sr and 34 sr, the maximum being reached around -50°C . Overall, this corresponds to a mean value of 34.7 sr and a median value of 33.1 sr.

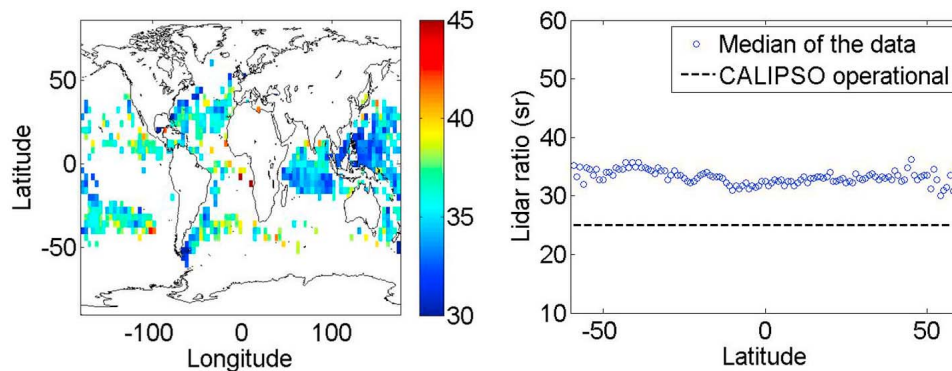


Figure 8. (left) Map of lidar ratio as retrieved by combining SODA and CALIPSO integrated attenuated backscatter coefficient. (right) Latitudinal variation of the lidar ratio distribution.

The minimum value, about 30 sr, is observed at the coldest temperatures (-70°C), consistently with Figure 8.

7.2. Discussion

[45] We will make a preliminary analysis of the derived data, in order to compare with results from earlier studies, and discuss campaigns performed on cirrus clouds close to the Pacific area, in Central America, as well as some early results using CALIOP data. Further reduction of error sources (mainly coming from aerosol contamination) would be needed prior to providing a more comprehensive analysis and this is beyond the scope of this first study on the application of ocean surface echo for cirrus cloud properties analysis. We will refer here to the lidar ratio, S , as introduced by equation (9). Different authors [Platt *et al.*, 1980; Baum *et al.*, 2010] use different formalisms to represent the same quantity (like backscatter phase function). When this is the case, those formalisms have been converted to be consistent with equation (9).

[46] As reported in Figure 8, S shows some level of geographical variations and smaller than average values of the lidar ratio are observed over Indonesia. In a previous study [Baum *et al.*, 2010] based on 1 year (2008) of CALIOP data, geographical variations of the lidar ratio were already observed for dense clouds. The average lidar ratio for opaque cirrus clouds has been found over ocean to be somewhat lower (S between 26 and 29 sr over ocean for $\eta = 0.6$) than the one retrieved here. Note that in the work of Baum *et al.* [2010], continental and oceanic cirrus exhibit different properties, with lidar ratio values over land being somewhat smaller (25 sr).

[47] The lidar ratio as retrieved by the direct transmittance method for 1 year (2010) of nighttime data only over land is 30.0 ± 7.5 sr, which is $\sim 10\%$ lower than what we retrieve using SODA over the ocean (33 sr) but higher than what was retrieved for dense clouds. This seems to suggest that when the analysis is limited to the same type of cloud (either dense or semitransparent single-layer cirrus) the lidar ratio is slightly lower over land than over ocean. However, dense and semitransparent cirrus may have different properties. Further research will have to be conducted to know if this difference between dense and semitransparent single-layer cirrus comes from instrumental reasons linked to a higher amount of multiple scattering in dense clouds or if there are real geophysical variations.

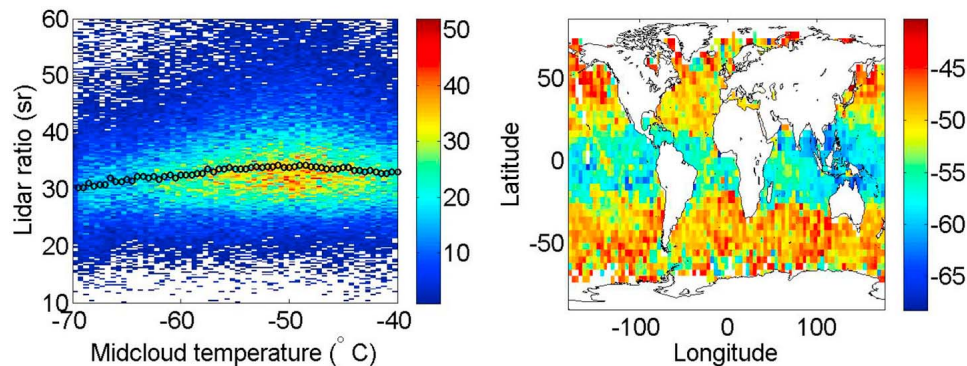


Figure 9. (left) Lidar ratio as retrieved using equation (9) as a function of midcloud temperature. Distribution of all observations for 1 year of data (2010) for daytime, single-layer semitransparent cirrus (scene type 21 in the IIR classification). Color code is the logarithm of the number of observations. Superimposed on the same image is the median of the data. (right) The map of average midcloud temperature of the clouds studied here.

[48] In their paper related to observations acquired during the Maritime Continent Thunderstorm Experiment (MCTEX) close to Australia, PL02 used the LIRAD method to retrieve the lidar ratio in tropical cirrus clouds. After applying corrections using in situ measurements, they retrieved lidar ratios much larger than ours, with values ranging from 42 to 74 sr ($k = 0.30$ and 0.17 sr^{-1} , respectively) for temperatures between -45°C and -70°C , respectively. Values of the ratio of visible to IR optical depths (called α in PL02 and identified as $1/BA_D$ in section 2) were determined from a fit to lidar integrated attenuated backscatter versus emissivity data. Those values were much larger than the ones used here. However, using in situ probes they also measured small particles with diameters smaller than $20 \mu\text{m}$, which we do not observe here using the IIR retrieval, although the IIR has the sensitivity to detect such particles in the clouds selected here (Garnier et al., submitted manuscript, 2011). The in situ measurements may have been affected by shattering [Field et al., 2006], but this would not affect the lidar and radiometry optical depth ratio. In the previous ARM-PROBE experiment part of the TOCA-COARE campaign, Platt et al. [1998] also found lidar ratio values higher than our results.

[49] Several other studies report values somewhat lower than ours. From ground-based measurements over Taiwan, Chen et al. [2002] derived a mean value of 29 sr. Using observations by the Cloud Physics Lidar (CPL) made largely over or in close proximity to North America, Yorks et al. [2011] determined a mean cirrus lidar ratio of 25 sr, and this value is very similar to that obtained from analyses of ground-based high spectral resolution lidar measurements [Holz, 2002].

[50] While the values found in these various field experiments differ from ours, it should be noted that we have analyzed only a very specific high-quality subset of the available data, consisting solely of single-layer clouds with a restricted range of optical depths embedded in otherwise clear skies. Enforcement of this data selection criterion may lead to significant differences in terms of microphysical and optical properties when our results are compared to other data sets.

[51] Furthermore, we have analyzed a truly global data set over a full 1 year time span, whereas field campaigns are

typically conducted over limited geographic areas and for limited temporal durations. The differences between our results and those from various field campaigns can thus be readily explained if the cirrus over the studied areas were not representative of our observations. As yet, there is no ground-based network or airborne system which can provide an annual data set on a global scale, especially over the oceans. It has also to be kept in mind that, as discussed in section 5.2, the multiple scattering factor in CALIOP seems to be stable (at least for the semitransparent cirrus considered in this study) and this may not be the case for a ground-based or airborne lidar system, which would complicate the retrievals (and comparisons) of the real lidar ratios.

[52] In a more recent paper, CALIOP data were analyzed over high dense cloud in the Pacific warm pool [Platt et al., 2011, hereinafter PL11]. Values of the lidar ratio more comparable with our analysis were obtained using the CALIOP operational multiple scattering factor ($\eta = 0.6$). What is interesting, however, is the variation of the lidar ratio S observed in and close to the convective core of the mesoscale convective system observed. Values as low as $S = 14$ sr were obtained in the opaque updraft, whereas much larger values were measured outside increasing to $S = 30$ sr in the semitransparent regions. Extreme values at -80°C were varied between 26 and 14 sr. On the basis of collocated CloudSat data, these low values are seen to correspond to a narrow updraft region where smaller effective radii extended up to the top of the cloud. One should further notice that relating smaller values of S (large values of the phase function) to lower temperatures and smaller crystal size as by [Platt et al., 2011], is opposite to previous analyses from field experiments as analyzed from in situ probes [Platt et al., 1998, 2002], but these last observations were not performed near the top of active convective cores. However, the [Platt et al., 2011] findings are more consistent with the S , temperature and size variations observed from SODA and IIR analysis for semitransparent clouds, as well as the decrease in the ηS product seen in Figure 2 for lower transmission (higher optical depths).

[53] If, as discussed by [Platt et al., 2011] and our results (Figure 9), the lidar ratio is weakly variable as a function of temperature, those slight variations can explain the geographical variations over Indonesia with respect to other

regions, as cirrus layers are frequently observed at high altitudes and low temperatures in the high troposphere. This region is well known as a deep convection area, and convective turrets are frequently seen to reach altitudes of 18 km (-70 to -80°C) [Platt *et al.*, 1998; Meenu *et al.*, 2010]. This activity leads to the more frequent elevated cloud layers observed in this area. Convection may also be a link to the smaller values of S observed in cirrus clouds over land.

[54] Although there seems to be a link between temperature and lidar ratio, possible changes in cirrus cloud properties due to change in nucleation processes cannot be ruled out in this preliminary analysis. There are more diatoms in the southern hemisphere ocean [Alvain *et al.*, 2008], and they have been shown to stimulate ice nucleation at low temperature [Knopf *et al.*, 2010] which could in turn lead to different properties of ice crystals and the higher than average lidar ratio reported in Figure 9. Slightly larger particle sizes are also observed in the IIR operational V3 data in these areas.

[55] It is important to stress that the variability we discuss occurs within the context of a high average stability of the lidar ratio. The order of magnitude of the average lidar ratio variations we found is around 10% when specific clouds are selected (single-layer ice clouds), and a very large number of data samples is considered (on the order of 100,000 for this study). Overall, the lidar ratio is stable even if it shows slight variations as a function of latitude and/or temperature.

[56] This indicates the current approach adopted in the CALIOP operational “inversion” procedure of using a single lidar ratio and a single multiple scattering coefficient is at first order valid for semitransparent cirrus. However, the value of the lidar ratio would have to be revisited in order to be consistent with SODA (and to be statistically self consistent with the “direct transmission” algorithm). In term of perspective, this work also prepare the way for future studies dedicated to use the combined radar and lidar vertical profiles along with the infrared observations to better estimate the radiative impact of cirrus clouds. The knowledge of the absolute column optical depth and mean lidar ratio as well as mean multiple scattering coefficient, offers a constraint to improve the retrieval of the optical properties of thin ice clouds (single or multiple layers) on the vertical and better estimate their interaction with solar and terrestrial infrared radiation.

8. Conclusion

[57] We have presented the results from the integrated approach using CALIPSO/CloudSat ocean surface echo to retrieve the optical depth of single-layer semitransparent cirrus clouds over oceans. The retrieved optical depths are shown to be consistent with the ones derived in the infrared from the IIR with respect to theoretical calculations. Following previous analyses, the combination of SODA and IIR lead to results consistent with the value of the multiple scattering used in the operational analysis. However, the operational lidar ratio is found to be biased low by about 25%, and thus the CALIOP cirrus optical depths are likewise underestimated in the version 3 data products. The analysis of such properties of cirrus clouds, at the global scale showed more homogeneous results than previously derived from field experiments. These results stress the strong

potential of the method using ocean surface scattering. It is promising for future research focused on retrieving optical depth when multilayer features are present.

[58] From our results on single-layer elevated ice clouds, Indonesia was identified as a region exhibiting smaller values of the lidar ratio. These values were seen to correspond to the coldest temperatures, where small particle sizes were observed by the IIR in the semitransparent cloud layers. This behavior is consistent with the larger occurrence of convective turrets in this area and with similar lidar ratios observed in and near the convective cores. This is also consistent with smaller values of the particle sizes retrieved from satellite in these cores. Future work needs to be conducted to further investigate the underlying physical mechanisms.

[59] **Acknowledgments.** The CALIPSO mission is a joint NASA-CNES program. Both agencies are acknowledged for their support of this study. CloudSat and AMSR-E projects are greatly acknowledged for data availability. Science System and Application Inc. (SSAI) is greatly acknowledged for its support. SODA project is developed at ICARE data center (<http://www.icare.univ-lille1.fr/>) in Lille (France), which is greatly acknowledged for technical support and skill in data collocation. We would like to thank M. Platt for fruitful discussions in the frame of the CALIPSO mission and the three anonymous reviewers for their helpful comments.

References

- Alvain, S., C. Moulin, Y. Dandonneau, and H. Loisel (2008), Seasonal distribution and succession of dominant phytoplankton groups in the global ocean: A satellite view, *Global Biogeochem. Cycles*, 22, GB3001, doi:10.1029/2007GB003154.
- Barrick, D. E. (1968), Rough surface scattering based on the specular point theory, *IEEE Trans. Antennas Propag.*, 16(4), 449–454, doi:10.1109/TAP.1968.1139220.
- Baum, B. A., P. Yang, A. J. Heymsfield, S. Platnick, M. D. King, Y.-X. Hu, and S. T. Bedka (2005), Bulk scattering properties for the remote sensing of ice clouds. Part II: Narrowband models, *J. Appl. Meteorol.*, 44, 1896–1911, doi:10.1175/JAM2309.1.
- Baum, B. A., P. Yang, Y. Hu, and Q. Feng (2010), The impact of ice particle roughness on the scattering phase matrix, *J. Quant. Spectrosc. Radiat. Transfer*, 111, 2534–2549, doi:10.1016/j.jqsrt.2010.07.008.
- Baum, B. A., P. Yang, A. J. Heymsfield, C. G. Schmitt, Y. Xie, A. Bansemmer, Y.-X. Hu, and Z. Zhang (2011), Improvements in shortwave bulk scattering and absorption models for the remote sensing of ice clouds, *J. Appl. Meteorol. Climatol.*, 50, 1037–1056, doi:10.1175/2010JAMC2608.1.
- Bissonnette, L. R. (1996), Multiple-scattering lidar equation, *Appl. Opt.*, 35, 6449–6465, doi:10.1364/AO.35.006449.
- Bohren, C. F., and D. R. Huffman (1983), *Absorption and Scattering of Light by Small Particles*, John Wiley, New York.
- Br on, F. M., and N. Henriot (2006), Spaceborne observations of ocean glint reflectance and modeling of wave slope distributions, *J. Geophys. Res.*, 111, C06005, doi:10.1029/2005JC003343.
- Bufton, J. L., F. E. Hoge, and R. N. Swift (1983), Airborne measurements of laser backscatter from the ocean surface, *Appl. Opt.*, 22, 2603–2618, doi:10.1364/AO.22.002603.
- Chen, W. N., C.-W. Chiang, and J.-B. Nee (2002), Lidar ratio and depolarization ratio for cirrus clouds, *Appl. Opt.*, 41, 6470–6476, doi:10.1364/AO.41.006470.
- Chepfer, H., J. Pelon, G. Brogniez, C. Flamant, V. Trouillet, and P. H. Flamant (1999), Impact of cirrus cloud ice crystal shape and size on multiple scattering effects: Application to spaceborne and airborne backscatter lidar measurements during LITE mission and E-LITE campaign, *Geophys. Res. Lett.*, 26, 2203–2206, doi:10.1029/1999GL900474.
- Cox, C., and W. Munk (1954), Measurement of the roughness of the sea surface from photographs of the Sun’s glitter, *J. Opt. Soc. Am.*, 44(11), 838–850, doi:10.1364/JOSA.44.000838.
- Eloranta, E. W. (1998), A practical model for the calculation of multiply scattered lidar returns, *Appl. Opt.*, 37, 2464–2472, doi:10.1364/AO.37.002464.
- Fernald, F. G., B. M. Herman, and J. A. Reagan (1972), Determination of aerosol height distribution by lidar, *Appl. Opt.*, 11, 482–489.
- Field, P. R., A. J. Heymsfield, and A. Bansemmer (2006), Shattering and particle interarrival times measured by optical array probes in ice clouds, *J. Atmos. Oceanic Technol.*, 23, 1357–1371, doi:10.1175/JTECH1922.1.

- Fu, Q., and K.-N. Liou (1993), Parameterization of the radiative properties of cirrus clouds, *J. Atmos. Sci.*, **50**, 2008–2025, doi:10.1175/1520-0469(1993)050<2008:POTRPO>2.0.CO;2.
- Heymsfield, A. J., and L. M. Miloshevich (2003), Parameterizations for the cross-sectional area and extinction of cirrus and stratiform ice cloud particles, *J. Atmos. Sci.*, **60**, 936–956, doi:10.1175/1520-0469(2003)060<0936:PFTCSA>2.0.CO;2.
- Hogan, R. J. (2008), Fast lidar and radar multiple-scattering models. Part I: Small-angle scattering using the photon variance-covariance method, *J. Atmos. Sci.*, **65**, 3621–3635, doi:10.1175/2008JAS2642.1.
- Holz, R. E. (2002), Measurements of cirrus backscatter phase functions using a high spectral resolution lidar, M.S. thesis, Dep. of Atmos. and Oceanic Sci., Univ. of Wis.-Madison, Madison, May.
- Hu, Y., et al. (2009), CALIPSO/CALIOP cloud phase discrimination algorithm, *J. Atmos. Oceanic Technol.*, **26**, 2293–2309, doi:10.1175/2009JTECHA1280.1.
- Huang, J., P. Minnis, B. Lin, T. Wang, Y. Yi, Y. Hu, S. Sun-Mack, and K. Ayers (2006), Possible influences of Asian dust aerosols on cloud properties and radiative forcing observed from MODIS and CERES, *Geophys. Res. Lett.*, **33**, L06824, doi:10.1029/2005GL024724.
- Ivanova, D., D. L. Mitchell, W. P. Arnott, and M. Poellot (2001), A GCM parameterization for bimodal size spectra and ice mass removal rates in mid-latitude cirrus clouds, *Atmos. Res.*, **59–60**, 89–113, doi:10.1016/S0169-8095(01)00111-9.
- Jackson, F. C., W. T. Walton, D. E. Hines, B. A. Walter, and C. Y. Peng (1992), Sea surface mean square slope from Ku-Band backscatter data, *J. Geophys. Res.*, **97**, 11411–11427, doi:10.1029/92JC00766.
- Joint Committee for Guides in Metrology (2008), Evaluation of measurement data: Guide to the expression of uncertainty in measurement, *Rep. JCGM 100:2008*, Bur. Int. des Poids et Mes., Sèvres, France.
- Josset, D., J. Pelon, A. Protat, and C. Flamant (2008), New approach to determine aerosol optical depth from combined CALIPSO and CloudSat ocean surface echoes, *Geophys. Res. Lett.*, **35**, L10805, doi:10.1029/2008GL033442.
- Josset, D., J. Pelon, and Y. Hu (2010a), Multi-instrument calibration method based on a multiwavelength ocean surface model, *IEEE Geosci. Remote Sens. Lett.*, **7**, 195–199, doi:10.1109/LGRS.2009.2030906.
- Josset, D., P.-W. Zhai, Y. Hu, J. Pelon, and P. L. Lucker (2010b), Lidar equation for ocean surface and subsurface, *Opt. Express*, **18**, 20862–20875, doi:10.1364/OE.18.020862.
- Klett, J. D. (1981), Stable analytical inversion solution for processing lidar returns, *Appl. Opt.*, **20**, 211–220, doi:10.1364/AO.20.000211.
- Knopf, D. A., P. A. Alpert, B. Wang, and J. Y. Aller (2010), Stimulation of ice nucleation by marine diatoms, *Nat. Geosci.*, **4**, 88–90, doi:10.1038/ngeo1037.
- Labonnote, C. L., G. Brogniez, M. Doutriaux-Boucher, J. Buriez, J. Gayet, and H. Chepfer (2000), Modeling of light scattering in cirrus clouds with inhomogeneous hexagonal monocrystals: Comparison with in-situ and ADEOS-POLDER measurements, *Geophys. Res. Lett.*, **27**, 113–116, doi:10.1029/1999GL010839.
- Lamquin, N., C. J. Stubenrauch, and J. Pelon (2008), Upper tropospheric humidity and cirrus geometrical and optical thickness: Relationships inferred from one year of collocated AIRS and CALIPSO data, *J. Geophys. Res.*, **113**, D00A08, doi:10.1029/2008JD010012.
- Lhermitte, R. (1987), A 94-GHz Doppler radar for cloud observations, *J. Atmos. Oceanic Technol.*, **4**, 36–48, doi:10.1175/1520-0426(1987)004<0036:AGDRFC>2.0.CO;2.
- Li, L., G. M. Heymsfield, L. Tian, and P. E. Racette (2005), Measurements of ocean surface backscattering using an airborne 94-GHz cloud radar: Implication for calibration of airborne and spaceborne W-band radars, *J. Atmos. Oceanic Technol.*, **22**, 1033–1045, doi:10.1175/JTECH1722.1.
- Liu, Y., M. Y. Su, X. H. Yan, and W. T. Liu (2000), The mean-square slope of ocean surface waves and its effect on radar backscatter, *J. Atmos. Oceanic Technol.*, **22**, 1033–1045.
- Meenu, S., K. Rajeev, K. Parameswaran, and A. K. M. Nair (2010), Regional distribution of deep clouds and cloud top altitudes over the Indian subcontinent and the surrounding oceans, *J. Geophys. Res.*, **115**, D05205, doi:10.1029/2009JD011802.
- Menzies, R. T., D. M. Tratt, and W. H. Hunt (1998), Lidar in-space technology experiment measurements of sea surface directional reflectance and the link to surface wind speed, *Appl. Opt.*, **37**, 5550–5559, doi:10.1364/AO.37.005550.
- Minnis, P., K. N. Liou, and Y. Takano (1993), Inference of cirrus cloud properties using satellite-observed visible and infrared radiances. Part I: Parameterization of radiance fields, *J. Atmos. Sci.*, **50**, 1279–1304, doi:10.1175/1520-0469(1993)050<1279:IOCCPU>2.0.CO;2.
- Mishchenko, M. I., L. D. Travis, and A. A. Lacis (2002), *Scattering, Absorption, and Emission of Light by Small Particles*, Cambridge Univ. Press, Cambridge, U. K.
- Mitchell, D. L., S. Chai, Y. Liu, A. J. Heymsfield, and Y. Y. Dong (1996), Modeling cirrus clouds. Part I: Treatment of bimodal size spectra and case study analysis, *J. Atmos. Sci.*, **53**, 2952–2966, doi:10.1175/1520-0469(1996)053<2952:MCCPIT>2.0.CO;2.
- Phillips, O. M. (1977), *The Dynamic of the Upper Ocean*, 2nd ed., Cambridge Univ. Press, Cambridge, U. K.
- Platnick, S., M. D. King, S. A. Ackerman, W. P. Menzel, B. A. Baum, J. C. Riédi, and R. A. Frey (2003), The MODIS cloud products: Algorithms and examples from Terra, *IEEE Trans. Geosci. Remote Sens.*, **41**, 459–473, doi:10.1109/TGRS.2002.808301.
- Platt, C. M. R. (1973), Lidar and radiometric observations of cirrus clouds, *J. Atmos. Sci.*, **30**, 1191–1204, doi:10.1175/1520-0469(1973)030<1191:LAROOC>2.0.CO;2.
- Platt, C. M. R., D. W. Reynolds, and N. L. Abshire (1980), Satellite and lidar observations of the albedo, emittance and optical depth of cirrus compared to model calculations, *Mon. Weather Rev.*, **108**, 195–204.
- Platt, C. M. R., S. A. Young, P. J. Manson, G. R. Patterson, S. C. Marsden, R. T. Austin, and J. Churnside (1998), The optical properties of equatorial cirrus from observations in the ARM Pilot Radiation Observation Experiment, *J. Atmos. Sci.*, **55**, 1977–1996, doi:10.1175/1520-0469(1998)055<1977:TOPOEC>2.0.CO;2.
- Platt, C. M. R., S. A. Young, R. T. Austin, G. R. Patterson, D. L. Mitchell, and S. D. Miller (2002), LIRAD observations of tropical cirrus clouds in MCTEX. Part I: Optical properties and detection of small particles in cold cirrus, *J. Atmos. Sci.*, **59**, 3145–3162, doi:10.1175/1520-0469(2002)059<3145:LOOTCC>2.0.CO;2.
- Platt, C. M. R., M. A. Vaughan, and R. T. Austin (2011), Characteristics of CALIPSO and CloudSat backscatter at the top center layers of mesoscale convective systems and relation to cloud microphysics, *J. Appl. Meteorol. Climatol.*, **50**, 368–378, doi:10.1175/2010JAMC2537.1.
- Powell, K. A., M. A. Vaughan, R. R. Rogers, R. E. Kuehn, W. H. Hunt, K.-P. Lee, and T. D. Murray (2010), The CALIOP 532-nm channel daytime calibration: Version 3 algorithm, paper presented at 25th International Laser Radar Conference, Int. Coord. Group on Laser Atmos. Stud., St. Petersburg, Russia.
- Rogers, R. R., et al. (2011), Assessment of the CALIPSO lidar 532 nm attenuated backscatter calibration using the NASA LaRC airborne High Spectral Resolution Lidar, *Atmos. Chem. Phys.*, **11**, 1295–1311, doi:10.5194/acp-11-1295-2011.
- Sassen, K., and J. M. Comstock (2001), A midlatitude cirrus cloud climatology from the facility for atmospheric remote sensing. Part III: Radiative properties, *J. Atmos. Sci.*, **58**, 2113–2127, doi:10.1175/1520-0469(2001)058<2113:AMCCCF>2.0.CO;2.
- Stephens, G. L., et al. (2008), CloudSat mission: Performance and early science after the first year of operation, *J. Geophys. Res.*, **113**, D00A18, doi:10.1029/2008JD009982.
- Tanelli, S., S. L. Durden, E. Im, K. S. Pak, D. G. Reinke, P. Partain, J. M. Haynes, and R. T. Marchand (2008), CloudSat's Cloud Profiling Radar after two years in orbit: Performance, calibration, and processing, *IEEE Trans. Geosci. Remote Sens.*, **46**, 3560–3573, doi:10.1109/TGRS.2008.2002030.
- Valenzuela, G. R. (1970), The effective reflection coefficients in forward scattering from a dielectric slightly rough surface, *Proc. IEEE*, **58**, 1279, doi:10.1109/PROC.1970.7902.
- Valenzuela, R. G. (1978), Theories for the interaction of electromagnetic and oceanic waves: A review, *Boundary Layer Meteorol.*, **13**, 61–85, doi:10.1007/BF00913863.
- Vernier, J. P., et al. (2009), Tropical stratospheric aerosol layer from CALIPSO lidar observations, *J. Geophys. Res.*, **114**, D00H10, doi:10.1029/2009JD011946.
- Vernier, J.-P., et al. (2011), Major influence of tropical volcanic eruptions on the stratospheric aerosol layer during the last decade, *Geophys. Res. Lett.*, **38**, L12807, doi:10.1029/2011GL047563.
- Winker, D. M. (2003), Accounting for multiple scattering in retrievals from space lidar, *Proc. SPIE*, **5059**, 128–139, doi:10.1117/12.512352.
- Winker, D. M., M. A. Vaughan, A. Omar, Y. Hu, K. A. Powell, Z. Liu, W. H. Hunt, and S. A. Young (2009), Overview of the CALIPSO mission and CALIOP data processing algorithms, *J. Atmos. Oceanic Technol.*, **26**, 2310–2323, doi:10.1175/2009JTECHA1281.1.
- Winker, D. M., et al. (2010), The CALIPSO mission: A global 3D view of aerosols and clouds, *Bull. Am. Meteorol. Soc.*, **91**, 1211–1229, doi:10.1175/2010BAMS3009.1.
- Xie, Y., P. Yang, G. W. Kattawar, P. Minnis, and Y. X. Hu (2009), Effect of the inhomogeneity of ice crystals on retrieving ice cloud optical thickness and effective particle size, *J. Geophys. Res.*, **114**, D11203, doi:10.1029/2008JD012116.
- Yang, P., G. Hong, G. W. Kattawar, P. Minnis, and Y. X. Hu (2008a), Uncertainties associated with the surface texture of ice particles in satellite-based retrieval of cirrus clouds: Part II. Effect of particle surface roughness on retrieved cloud optical thickness and effective particle size,

- IEEE Trans. Geosci. Remote Sens.*, 46, 1948–1957, doi:10.1109/TGRS.2008.916472.
- Yang, P., G. W. Kattawar, G. Hong, P. Minnis, and Y. X. Hu (2008b), Uncertainties associated with the surface texture of ice particles in satellite-based retrieval of cirrus clouds: Part I. Single-scattering properties of ice crystals with surface roughness, *IEEE Trans. Geosci. Remote Sens.*, 46, 1940–1947, doi:10.1109/TGRS.2008.916471.
- Yorks, J. E., D. L. Hlavka, W. D. Hart, and M. J. McGill (2011), Statistics of cloud optical properties from airborne lidar measurements, *J. Atmos. Oceanic Technol.*, 28, 869–883, doi:10.1175/2011JTECHA1507.1.
- Young, S. A. (1995), Analysis of lidar backscatter profiles in optically thin clouds, *Appl. Opt.*, 34, 7019–7031, doi:10.1364/AO.34.007019.
- Young, S. A., and M. A. Vaughan (2009), The retrieval of profiles of particulate extinction from cloud-aerosol lidar infrared pathfinder satellite observations (CALIPSO) data: Algorithm description, *J. Atmos. Oceanic Technol.*, 26, 1105–1119, doi:10.1175/2008JTECHA1221.1.
- Yue, Q., and K. N. Liou (2009), Cirrus cloud optical and microphysical properties determined from AIRS infrared spectra, *Geophys. Res. Lett.*, 36, L05810, doi:10.1029/2008GL036502.
- Zhang, Z., P. Yang, G. Kattawar, J. Riedi, L. C. Labonnote, B. A. Baum, S. Platnick, and H.-L. Huang (2009), Influence of ice particle model on satellite ice cloud retrieval: Lessons learned from MODIS and POLDER cloud product comparison, *Atmos. Chem. Phys.*, 9, 7115–7129, doi:10.5194/acp-9-7115-2009.
- A. Garnier and J. Pelon, LATMOS, IPSL, Universite Paris VI, 4 Place Jussieu, F-75252 Paris CEDEX 05, France.
- Y. Hu and M. Vaughan, NASA Langley Research Center, MS 435, 21 Langley Blvd., Hampton, VA 23681, USA.
- D. Josset, P. Lucker, and P.-W. Zhai, Science Systems and Applications, Inc., 1 Enterprise Pkwy., Ste. 200, Hampton, VA 23666, USA. (dbjosset@gmail.com)
- R. Kuehn, CIMSS, University of Wisconsin-Madison, 1225 W. Dayton St., Madison, WI 53706, USA.